JOURNAL OF GEOPHYSICAL RESEARCH, VOL. 104, NO. C10, PAGES 23,443–23,458, OCTOBER 15, 1999

Shallow water currents during Hurricane Andrew

Timothy R. Keen

Naval Research Laboratory, Oceanography Division, Stennis Space Center, Mississippi

Scott M. Glenn

Institute of Marine and Coastal Sciences, Rutgers University, New Brunswick, New Jersey

Abstract. Oceanographic measurements are used in combination with a numerical model to examine the influence of stratification on shallow water currents during the directly forced stage of a tropical cyclone (Hurricane Andrew) on the continental shelf. The following stratification-dependent coastal processes are examined: (1) turbulent mixing, (2) coastally trapped waves, (3) near-inertial oscillations, and (4) upwelling and downwelling. Turbulent mixing was strong within 1 R_w (radius of maximum winds) of the storm track, and stratification was nearly destroyed. Turbulent mixing was weak at distances greater than 2 R_w. The dominant coastal wave was a barotropic Kelvin wave generated as the storm surge relaxed after landfall. Baroclinic near-inertial oscillations were dominant at the shelf break and occurred along with a barotropic response on the middle shelf. Downwelling-favorable flow developed east of the track prior to the storm peak, and upwelling-favorable flow evolved west of the track as the eye crossed the shelf. The idealized storm flow was modified by local barotropic and baroclinic pressure gradients on the shelf. Ocean circulation during Hurricane Andrew was hindcast using both stratified and unstratified three-dimensional numerical models. For areas within 1 R_w of the storm track, the unstratified model matched the observed currents better than the stratified model, partly because of errors in the initial stratification. At distances greater than 2 R_w the influence of stratification increases, and the unstratified model does not reproduce the observed upwelling-favorable flow.

1. Introduction

Tropical and extratropical cyclones are among the most important oceanographic influences on continental shelves. These severe storms function as the primary physical mechanism for cleaning and revitalizing coastal seas, and redistributing material delivered from the continental interior. Interest in tropical cyclone currents ranges from disaster preparation in coastal areas to understanding the stratigraphy of continental shelf sediments. It is thus important from scientific, engineering, and public policy perspectives to understand the oceanographic response on the continental shelf to these storms.

Tropical cyclones are much smaller than extratropical cyclones and follow less-predictable paths. This has made it difficult to study the oceanographic response on the continental shelf in detail. Nevertheless, they do occasionally pass near instruments, and some measurements have been made. *Harris* [1958] has compiled observed coastal water levels during historical tropical cyclones, and *Hazelworth* [1968] has discussed the temperature response of the coastal ocean to a number of hurricanes. It is more difficult to obtain current measurements. Consequently, the number of published data sets is small [*Murray*, 1970; *Smith*, 1978, 1980; *Forristall et al.*, 1977; *Hearn and Holloway*, 1990].

Numerical models are often used to study tropical cyclone flows on the shelf because of the difficulty of collecting observations at the right place and time. Because the dominant response in shallow water is barotropic, two-dimensional (barotropic) models have been widely used to study coastal tropical storm flows. One application is the prediction of the hurricane storm surge [e.g., *Blain*, 1997; *Blain et al.*, 1998]. Two-dimensional models have also been used to examine the generation and propagation of continental shelf waves [*Fandry and Steedman*, 1994; *Tang et al.*, 1997] and the effects of wave-enhanced bottom friction on storm flows [*Tang and Grimshaw*, 1996]. One-dimensional models can be embedded within barotropic models to simulate stratified and unstratified storm flows in both shallow and deep water [*Forristall et al.*, 1977; *Cooper and Pearce*, 1982; *Signorini et al.*, 1992]. Three-dimensional, primitive-equation numerical models with turbulence closure schemes have been applied successfully to a number of problems that do not require stratification [*Spaulding and Isaji*, 1987; *Hearn and Holloway*, 1990; *Keen and Slingerland*, 1993a, b].

Stratified numerical models are capable of reproducing the three-dimensional structure of shallow water storm currents, especially the generation of internal shelf waves. The effects

Paper number 1999JC900180.
0148-0227/99/1999JC900180$09.00

of stratification can be studied using two-layer models [e.g., *Forristall*, 1980; *Gordon*, 1982] and isopycnal models [*Cooper and Thompson*, 1989]. Stratified, three-dimensional primitive-equation models with turbulence closure have been used to demonstrate the response of the deep ocean and continental slope to a passing hurricane [e.g., *Greatbatch*, 1984; *Shay et al.*, 1990; *Shay and Chang*, 1997; *Niwa and Hibiya*, 1997].

Because of the short duration of storm passage and the capabilities of modern computers, it is reasonable to simulate coastal baroclinic flows during a hurricane at spatial scales of the order of the baroclinic Rossby radius. The sensitivity of a stratified, three-dimensional numerical model of shallow-water hurricane flow has been examined by *Keen and Glenn* [1998]. One of the most important factors affecting model accuracy with respect to shallow water currents was stratification.

In this paper, observations are used in combination with numerical models to evaluate the role of stratification in determining the structure of storm currents during the directly forced stage of the shelf response [*Fandry and Steedman*, 1994]. We demonstrate that stratification is important in determining the three-dimensional structure of regional, shallow water hurricane flows. Section 2 examines observations from the Louisiana continental shelf during Hurricane Andrew in August 1992. Section 3 discusses the results of both stratified and unstratified numerical models, which were used to simulate the storm flow on the shelf. The model results are compared in section 4 and used to examine several aspects of the shallow water currents not directly measured by the instrumentation.

2. Observations during Hurricane Andrew

After crossing the Florida peninsula, Hurricane Andrew entered the Gulf of Mexico at 1200 UT, August 24, 1992, and the eye made landfall 200 km southwest of New Orleans, Louisiana (Figure 1), at 0900 UT, August 26. The forward speed of the eye decreased steadily, from 9 m s^{-1}, when it first entered the Gulf of Mexico, to 4 m s^{-1} as it crossed the Louisiana continental shelf. As part of the Louisiana-Texas (LATEX) observation program, moorings on the Louisiana shelf and slope (Table 1) measured continuous time series of currents, temperature, and salinity. Wind speed and direction and surface-wave spectra were measured at National Data Buoy Center (NDBC) buoys and oil platforms. Two bottom pressure sensors were also operating near the coast. The full set of observations during Hurricane Andrew are discussed by *Cardone et al.* [1994] (hereinafter referred to as C94).

2.1. Hurricane Winds

The wind field during Hurricane Andrew was measured at 12 locations (see C94) which give a representative picture of its spatial and temporal variability. The radius to maximum winds R_w increased as the storm crossed the Gulf of Mexico, from 11 km to 40 km immediately before landfall. Bullwinkle platform (see Figure 1 for location) is located approximately 100 km west of the storm track. The observed wind speed (Figure 2a) exceeded 25 m s^{-1} at the storm peak and remained above 15 m s^{-1} for more than 12 hours afterward. The wind was originally from the east, but it rotated counterclockwise (CCW) to become southerly after the eye made landfall. The measured winds at Grand Isle (Figure 2b) were similar to those at Bullwinkle, but the maximum wind speed was less than 25 m s^{-1}. The wind speed remained above 20 m s^{-1} for a longer interval, however. The Grand Isle station is east of the storm track, and the wind vector rotated clockwise (CW) as the eye passed.

2.2. Turbulent Mixing in the Coastal Ocean

Time series of temperature and salinity during Hurricane Andrew are similar, and the present discussion will focus on temperature only (Figure 3). Note that the panels in Figure 3 are arranged schematically according to relative location (Figure 1), with the landward moorings at the top. The solid

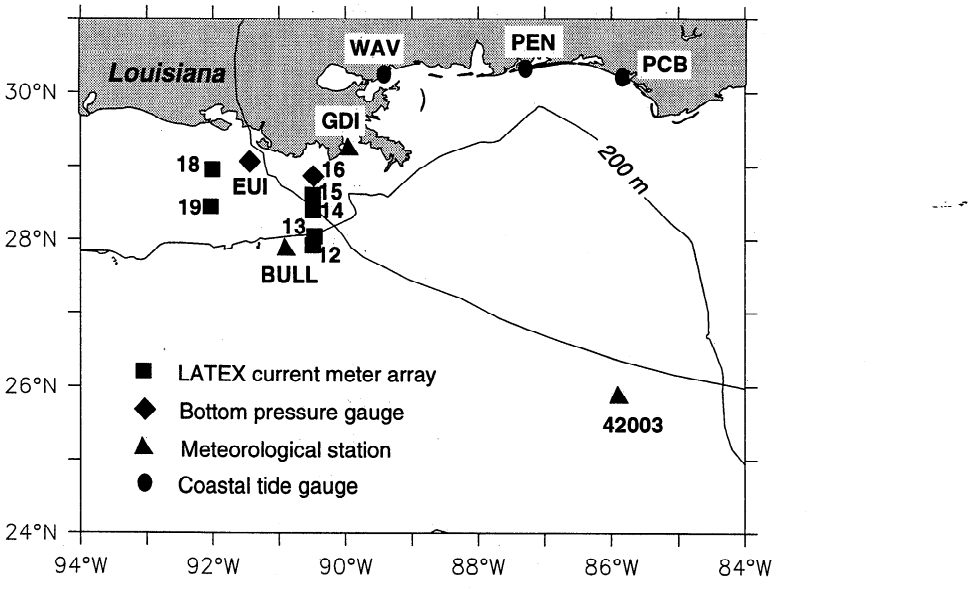

Figure 1. Detail map of northern Gulf of Mexico study area, showing storm path and moorings referred to in text. EUI, Eugene Island; BULL, Bullwinkle platform; 42003 is Buoy 42003; GDI, Grand Isle; PCB, Panama City Beach; PEN, Pensacola; and WAV, Waveland.

Table 1. Location of LATEX Current Meters for This Study

Mooring	Longitude	Latitude	Meter Depths, m	Water Depth, m
12	90.494598	27.923870	12, 100	505
13	90.485878	28.057529	12, 100, 190	200
14	90.492867	28.394569	11, 37	47
15	90.491577	28.608299	10, 17	20
18	91.982719	28.962730	10, 19	22
19	92.034798	28.465170	3, 47	51

lines in Figure 3 are the observations, and the dashed lines are model predictions, which are discussed in section 3.

The near-surface temperature on the middle and inner shelf was approximately 28°C before the storm. The temperature 3 m above the bed at moorings 15 and 18 (water depth approximately 20 m) was 22°C and 24.5°C, respectively. Although there is somewhat more variability in meter placement at moorings 14 and 19 (see Table 1), located near the 50 m isobath, the temperature difference is very similar at both. Near-bed temperatures are about 21°C at both moorings. The temperature at the upper meter at the shelf break (mooring 13) was slightly warmer than elsewhere on the shelf.

Mooring 18 is located approximately 2 R_w west of the storm track (on the left-hand side looking alongtrack), and consequently, the temperature response (Figure 3a) is weak. The near-surface temperature began to drop at 0000 UT, August 26, 6 hours before the eye passed. After decreasing by 2°C, a slight rebound occurred. The near-bottom temperature did not change until after the eye passed by, and there was no net change after the storm. These observations suggest that the mixed layer at this location did not reach the lower meter, which was at 19 m. The mixed-layer currents, represented by the upper current meter (Figure 4a), followed the wind direction closely during August 26, while bottom currents were shoreward.

Mooring 15 is about 1 R_w from the storm track, on the right-hand side of the hurricane, and its near-surface temperature (Figure 3b) indicates strong turbulent mixing before the instrument failed. The prestorm temperature difference was 7°C over a depth of 7 m. Temperature at the bottom increased by less than 3°C during the hurricane, however, and weak stratification persisted.

The surface temperature at mooring 19 (Figure 3c), located approximately 2.5 R_w west of the storm track, decreased by 1°C during the storm. The upper meter is only 3 m deep and may not be a good indicator of near-surface turbulent mixing, however. There is no evidence of turbulent mixing at the lower meter. This may be caused by the lower meter being 47 m below the surface. It may have been too deep to measure thermocline mixing.

The near-surface temperature at mooring 14 (Figure 3d) decreased 4°C before 0000 UT, August 26, when the hurricane eye passed directly over the mooring. The bottom temperature did not increase because turbulent mixing did not extend to a depth of 37 m. The surface temperature remained depressed during August 26, while the temperature at the lower meter fluctuated by as much as 4°C. Vertical current shear (Figure 4d) after 1000 UT was significant because of the persistent thermocline.

The temperature at the upper meter at mooring 13 (Figure 3e) began to drop at 1200 UT, August 24 when the wind speed at Bullwinkle (Figure 2a) was less than 10 m s^{-1}. This was the beginning of a steady decrease, which lasted until after the storm ended. By 0000 UT, August 27, the near-surface temperature had dropped almost 6°C.

Turbulent mixing was strongest at moorings closer than 1 R_w to the storm track. Thus mooring 14, which lay directly along the track, shows significant deepening of the mixed layer. Even here the water column was weakly stratified after the storm. A similar mixing history is indicated at mooring 15. Mooring 18 is about 2 R_w from the track and turbulent

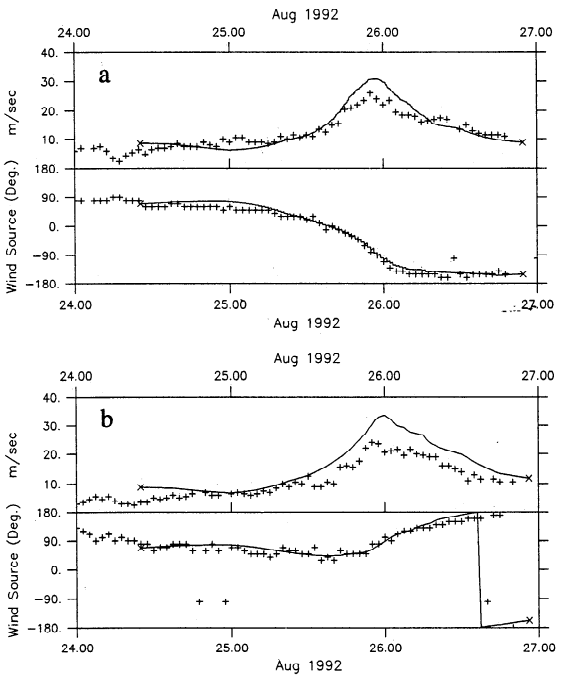

Figure 2. Time series of measured (pluses) and hindcast (line) wind speed (top panel) and direction (bottom panel) at (a) Bullwinkle Platform, and (b) Grand Isle.

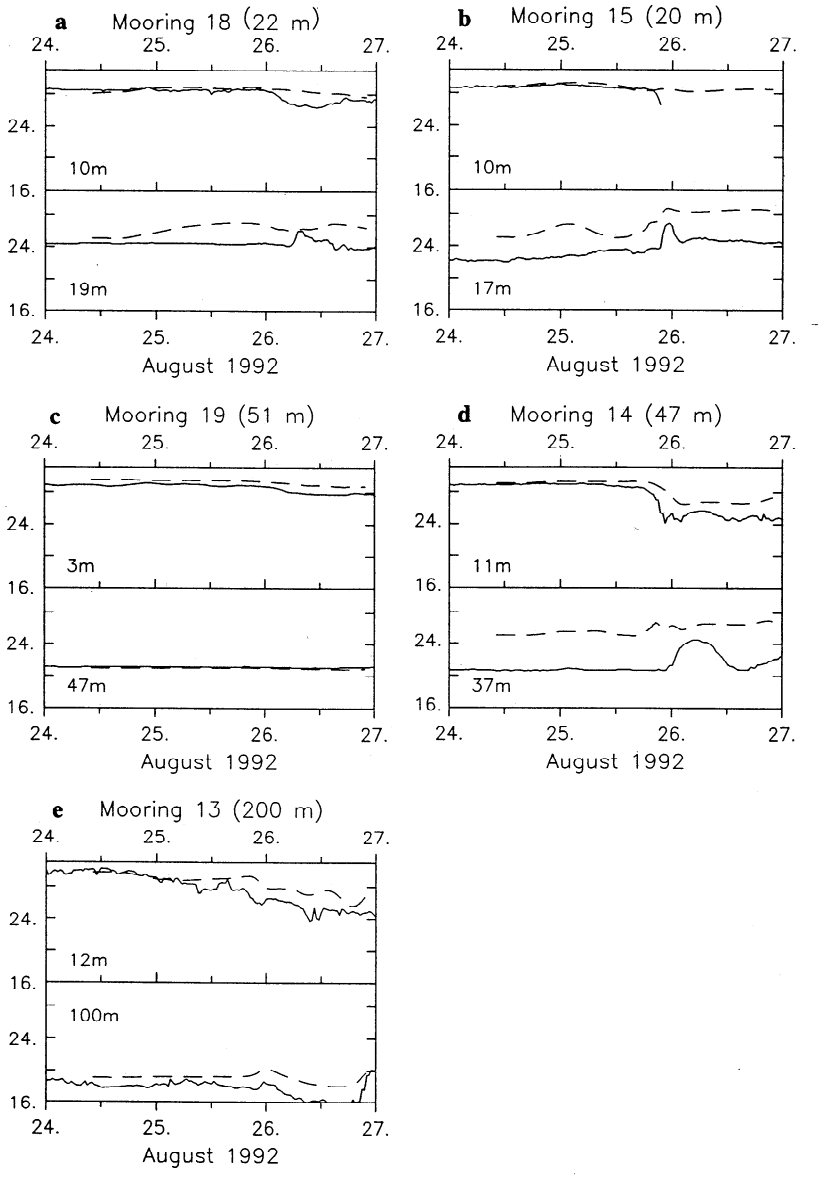

Figure 3. (a-e) Time series of measured (solid line) and hindcast (dashed line) temperatures at the Louisiana-Texas (LATEX) moorings listed in Table 1. See Figure 1 for locations.

mixing was much weaker. Finally, at approximately 2.5 R_w away, mooring 19 shows no significant effects of mixed-layer deepening.

2.3. Coastally Trapped Wave Response

It has been shown that the maximum transient response in shallow water is largely barotropic [e.g., *Fandry and Steedman*, 1994]. Thus it is useful to observe spatially distributed time series of water levels if possible. Water level measurements (Figure 5) from LATEX mooring 16, located approximately 2 R_w east of the storm track at the coast, and Eugene Isle, less than 1 R_w west of the track, are used. Water level observations from coastal tide stations are not discussed because these coastal locations do not measure water levels on the open shelf, and they are not accurately represented by the numerical models discussed in section 3.

Observed water levels at mooring 16 (squares in Figure 5) were steady until midday on August 25, when a storm surge forerunner arrived. The main storm surge developed in less than 10 hours and reached a maximum of 0.69 m at 0300 UT, August 26, before falling rapidly. The peak surge was only maintained for a few hours. Because of the rapidly changing coastal sea level, the shallow water barotropic response was transient. While sea level was increasing east of the storm track at the coast, currents at moorings 15 (Figure 4b) and 14 (Figure 4d) rotated to alongshelf. The coastal flow was geostrophic when the storm surge peaked.

Instead of being obliquely onshore, as on the eastern side of the storm track, the storm wind on the western side was offshore before August 26. This wind drove seaward flow at moorings 18 and 19. Consequently, the water level (Figure 5) at Eugene Isle fell to approximately −1 m before 0000 UT.

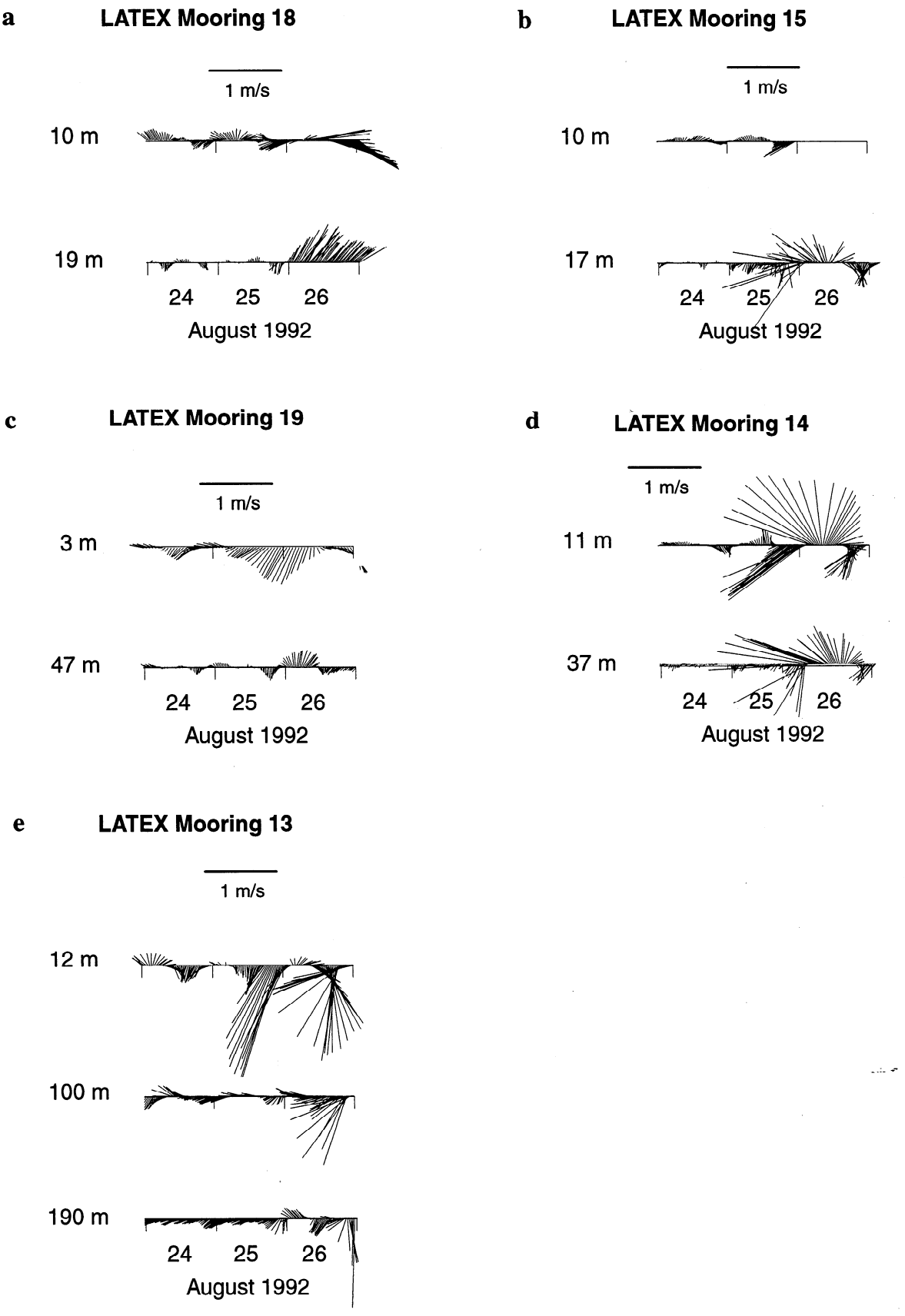

Figure 4. (a-e) Measured currents at the LATEX moorings listed in Table 1. See Figure 1 for locations. North is at top of page. The tic marks are at 0000 UT.

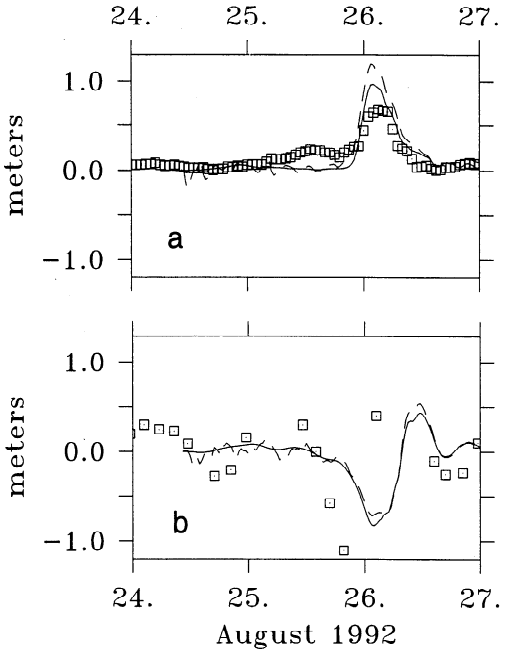

Figure 5. Time series of water levels (m) at (a) LATEX mooring 16 and (b) Eugene Isle. See Figure 1 for locations. Plus, measured; solid line, stratified model; dashed line, unstratified model.

Because of the incomplete record, however, it was not corrected for the astronomical tide, which had a predicted value of –0.2 m at this time (C94). The water level at Eugene Isle subsequently increased to more than 0.4 m sometime after 0300 UT.

The difference between the storm winds in left and right semicircles generated a coastal barotropic wave with a wavelength greater than 2.5 R_w before 0000 UT, August 26. If the storm surge maximum observed at mooring 16 propagated westward as a barotropic Kelvin wave, water levels at Eugene Isle, located 100 km west of mooring 16, would have reached a maximum after 0300 UT. A barotropic Kelvin wave with a speed of 14 m s^{-1} ($v = \sqrt{gh}$, where g is acceleration of gravity and h is average water depth of 20 m) would take about 2 hours to transit between mooring 16 and Eugene Isle. The observations are inadequate to determine the actual phase speed, however, because of the gap in the record at Eugene Isle. Furthermore, the alongshore propagation speed of the Kelvin wave is variable [*Fandry et al.*, 1984].

In addition to the barotropic Kelvin wave associated with the storm surge, continental shelf waves can be generated by a tropical cyclone wind stress field [*Tang et al.*, 1997]. Continental shelf waves generated by synoptic wind stresses have periods much greater than the inertial, wavelengths much larger than the shelf width, and amplitudes of the order of centimeters [*LeBlond and Mysak*, 1978]. In the present case, the generation mechanism may be relaxation of the storm-generated forced wave as the eye made landfall, as proposed for the generation of near-inertial-frequency internal waves on the shelf during hurricanes [*Cooper and Thompson*, 1989]. The presence of these subinertial vorticity waves is indicated by current meter records rather than by water levels. In the present study, it is not possible to use the current meters to identify the barotropic signal associated with continental shelf waves, because of the magnitude of the barotropic Kelvin wave and the short interval considered.

There is evidence in the temperature records of an internal Kelvin-wave front as discussed by *Crepon and Richez* [1982]. The near-bottom temperature at mooring 15 (Figure 3b) increased 4°C at the end of August 26 (no data are available for the upper meter). A similar increase was observed at mooring 14 (Figure 3d), with maximum amplitude occurring 5 hours later. A 2°C increase was also measured near the bottom at mooring 18 (Figure 3a) approximately 10 hours later than at mooring 15. No similar temperature change was recorded at mooring 19. These temperature perturbations may represent an internal wave front propagating from a point near mooring 15. Since mooring 18 is approximately 150 km west of mooring 15, the wave would have an along-shelf phase speed of about 4 m s^{-1}. Similarly, the across-shelf phase speed (between moorings 15 and 14) would be 1.3 m s^{-1}.

The internal-wave front at mooring 15 preceded the peak water level at mooring 16 by 4 hours. The internal wave recorded at mooring 18 followed the maximum storm surge at Eugene Isle by as much as 4 hours. The phase difference between external and internal waves increases with distance from the generation site because of the greater propagation speed of the external mode. Thus it is possible that both barotropic and baroclinic waves originated where the storm surge was a maximum, near mooring 16. The barotropic Kelvin wave then overtook the internal wave because it traveled about 5 times as fast.

2.4. Near-Inertial Response During Hurricane Andrew

A significant fraction of energy on the LATEX shelf is in the near-inertial band, with a period of 22-28 hours [*Chen et al.*, 1996; *Chen and Xie*, 1997]. Most of this near-inertial energy is associated with synoptic wind fields and the passage of cold fronts. The rare occurrence and short duration of hurricanes makes them insignificant to the overall energy distribution. Nevertheless, near-inertial oscillations excited within the region of storm winds contribute to coastal flows during hurricanes.

The temperature at a depth of 100 m at the shelf break (mooring 13) increased by 1°C (Figure 3e) at 2300 UT, August 25. The near-surface temperature also decreased slightly. This downward dislocation of the thermocline was preceded by mixed-layer currents (Figure 4e) greater than 1.5 m s^{-1}. Near-inertial currents were subsequently measured throughout the water column, appearing at all three current meters after one inertial period (IP). The currents at 100 m are correlated with a 4°C increase in temperature at the end of August 26.

Surface currents at mooring 14 (Figure 4d) indicate a mixed-layer origin of near-inertial oscillations on the middle shelf. Strong southwestward flow within the mixed layer at the end of August 25 is followed after 1 IP by southwest flow at both current meters, at which time the wind was blowing to the northeast. Bottom currents lagged the surface by approximately 2 hours. Bottom currents are similar at mooring 15 (Figure 14b). This near-inertial signal also had a barotropic component. The barotropic wave would have been reinforced by relaxation of the forced wave (storm surge) after landfall. These middle and inner-shelf flows lagged the near-inertial currents at the shelf break by approximately 6 hours.

The horizontal length scale for near-inertial oscillations is a useful metric for describing the spatial response of the LATEX shelf to wind forcing. *Cooper and Thompson* [1989] found a cross-shelf length scale of 300 km within the mixed layer for Hurricane Frederic. This is much greater than the length scale of approximately 80 km computed by *Chen et al.* [1996] using nonhurricane time series. Part of this discrepancy may arise from the numerical model of *Cooper and Thompson* [1989] being designed for the outer continental shelf and slope, whereas the analysis of *Chen et al.* [1996] included middle and inner shelf moorings. They found the along-shelf length scale to be 300-350 km.

The eastern and western LATEX arrays are 150 km apart and should have good coherence for the dominant synoptic forcing, but this distance is large compared to the storm scale R_w of 40 km. Consequently, the currents (Figure 4) at moorings 18 and 19 are very different from those at moorings 15 and 14, respectively. Currents at the eastern moorings are similar during the hurricane because the distance between moorings 13 and 15 (67 km) is close to the storm scale.

2.5. Upwelling- and Downwelling-Favorable Coastal Currents

If a steady wind blows parallel to a Northern Hemisphere coast with land to its right, a downwelling-favorable coastal flow regime will be established if the water column is stratified. An upwelling-favorable flow results if the coast is to the left of the wind. When a hurricane or extratropical cyclone approaches a coast at a high angle, the wind is parallel to the coast for extended periods, and a downwelling-favorable flow regime is expected [*Swift et al.*, 1986]. The horizontal length scale for Hurricane Andrew is of the order of 40 km, less than the shelf width. It is therefore likely that a more complex time-dependent coastal flow regime evolved which did not maintain this flow for extended intervals.

Flow at mooring 14 (Figure 4d) was downwelling-favorable before 1600 UT, August 25, after which the current direction was more uniform at both meters. The available observations at mooring 15 (Figure 4b) suggest that this flow regime was present there as well.

After 1200 UT, August 25, the flow at mooring 18 (Figure 4a) was offshore. As the wind rotated CCW to northwesterly, the coast was to the left of the wind and an upwelling-favorable flow developed. This flow continued through August 26. Surface currents at mooring 19 (Figure 4c) were consistently offshore throughout the storm, while bottom flow reversed direction after 0000 UT, August 26. This upwelling-favorable flow broke down 12 hours later.

3. Numerical Simulations

Three-dimensional flows during Hurricane Andrew were computed using the Princeton Ocean Model [*Mellor and Yamada*, 1982; *Oey and Chen*, 1992; *Mellor*, 1993]. As used for these simulations, the model includes wave-current bottom shear stresses [*Keen and Glenn*, 1994] and wave-breaking turbulence near the ocean surface [*Keen and Glenn*, 1998; *Craig and Banner*, 1994]. *Keen and Glenn* [1996; 1998] discuss several factors that influence the model's skill for predicting shallow water currents during Hurricane Andrew. The present simulations use the choice of model parameters (Table 2) that produced the best results in the previous work. The numerical model is integrated from 1000 UT, August 24, to 0000 UT, August 27, 1992. This interval is determined by the availability of validated hindcast wind and wave fields (C94). A sensitivity study of the integration time,

Table 2. Model Parameters

	Hindcast Values
Horizontal resolution: x, y	4885 m, 5559 m
Number σ Levels	20
Horizontal eddy viscosity parameter	0.1
Minimum depth	8 m
Maximum depth	3645 m
Wind, wave sources	hindcast fields: winds at 30 min. $C_D = 0.002$, waves at 1 hour
Horizontal boundary conditions	closed
Turbulence closure	Mellor-Yamada 2.5; breaking-wave turbulence within wave influenced layer
Bottom friction	neutral BBLM with bottom roughness computed: grain diameter = 1.56×10^{-4} m
Initial condition	$u = v$ = surface deviation = 0.0 stratified: salinity = 3-D depth dependent; temperature = 3-D depth dependent unstratified: salinity = 35; temperature = 20°C
Time step: internal, external	304.44 s, 10.15 s

before the storm wind stresses are applied, revealed that 1 to 2 days produced the best fit to the data from the moorings.

The Gulf of Mexico National Ocean Service (NOS) soundings were interpolated to the model domain (Figure 6a), with a minimum water depth of 8 m. The present study focuses on storm currents only. Therefore astronomical tides are neglected, and all lateral boundaries are closed. The study of *Keen and Glenn* [1998] revealed no significant improvement in skill for the hindcast interval using a full Gulf of Mexico domain.

To examine the influence of stratification on the shallow water currents during Hurricane Andrew, two numerical simulations have been completed. The first uses a three-dimensional initial condition for temperature and salinity. A hydrographic survey was completed between August 15 and 20, prior to Hurricane Andrew's passage. These profiles were compiled into depth-dependent temperature and salinity distributions (Figure 7). No heat or salt fluxes are applied at the surface. The second numerical simulation uses constant temperature and salinity. The numerical model is operated in three-dimensional prognostic mode for both cases.

The model-predicted flows are examined using maps of water surface deviations, surface currents, and bottom currents. The model currents from the σ levels are linearly interpolated to a depth of 1 m to represent surface currents. A logarithmic bottom boundary layer profile is used to interpolate the model currents to a height of 1 m above the bottom.

3.1. Stratified Model Results

3.1.1. Turbulent mixing. Errors in the initial temperature condition (Figure 3) influence model-predicted turbulent mixing. The largest error occurs at mooring 14, where the initial bottom temperature is more than 4°C high. An error of 3°C is present at mooring 15.

The stratified model reproduced the temperature histories at the moorings reasonably well (dashed lines in Figure 3), but the baroclinic response is clearly diminished. Model-predicted turbulent mixing is weak at the shelf break (Figure 3e), but the temperature history mimics the observations well. The final bottom-temperature change at mooring 14 is very close to the 1.5°C measured value. The temperature change at the surface is slightly low, however, suggesting insufficient mixing within the near-surface layer. The bottom temperature change at mooring 15 is 1°C high in the model. This suggests that the model actually mixed too much at this location. Errors in turbulent mixing at moorings 14 and 15 are partly attributable to the initial condition. The final change in temperature at the western moorings is very close to the observations.

3.1.2. Coastally trapped waves. The ability of the model to generate and propagate internal waves is strongly affected by the initial stratification. This is especially noticeable with respect to the internal wave front discussed in section 2.3. There is only a 2°C change at the bottom at mooring 14 (Figure 3d). The analogous wave at mooring 15 (Figure 3b) is

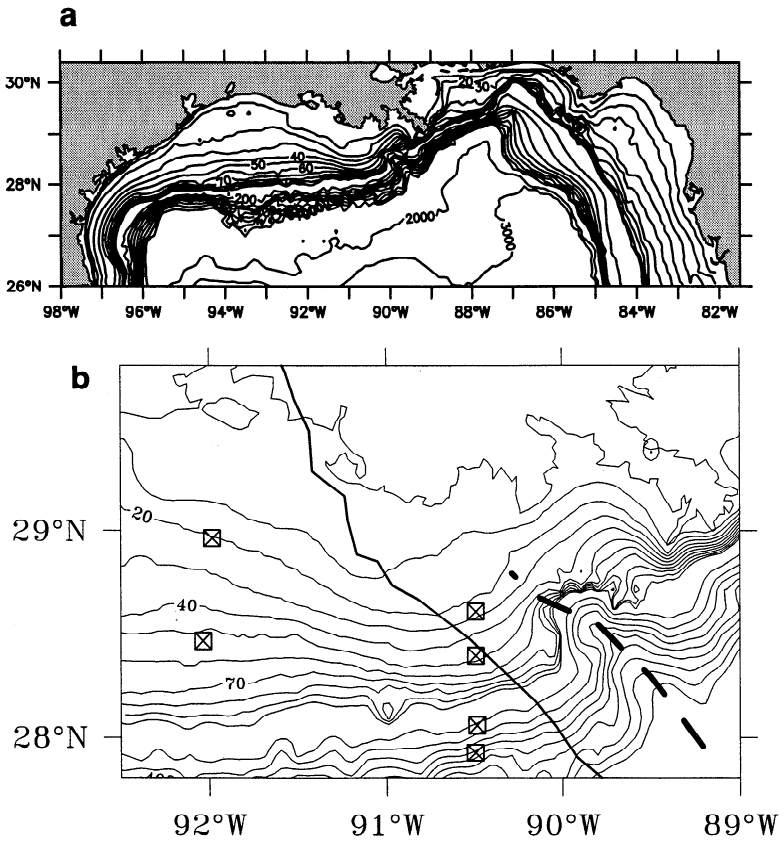

Figure 6. (a) Model bathymetry. Contour interval is 10 m from 0 to 100 m, 100m between 100 and 1000 m, and 1000 m from 1000 m to 3000 m. (b) Detail view of Louisiana study area. Mississippi Canyon is indicated by the dashed line in Figure 6b.

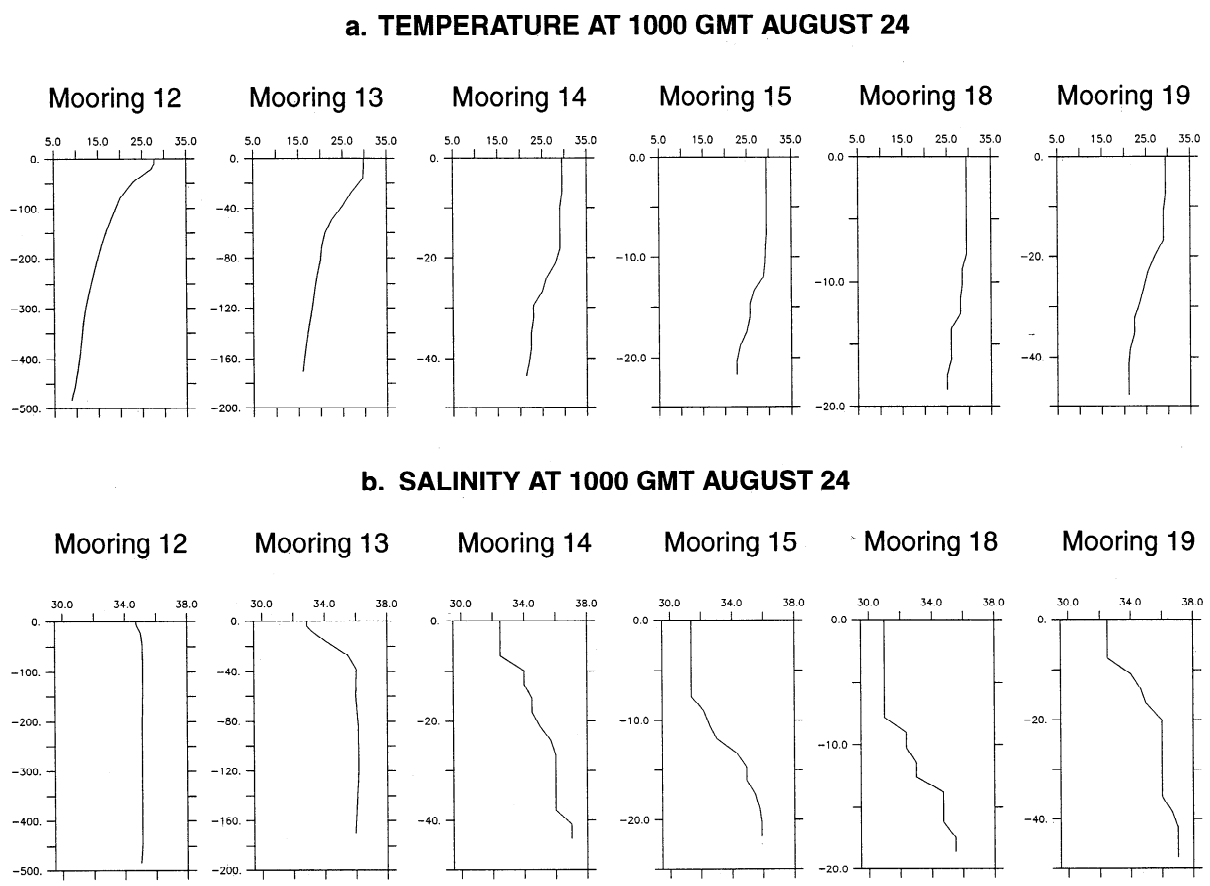

Figure 7. Profiles of (a) initial temperature and (b) initial salinity at all moorings used in stratified model.

also much weaker than observed. The observations indicate a similar baroclinic wave at mooring 18 (Figure 3a), which is not predicted by the model. Instead, the model generates an earlier internal wave with amplitude 2°C. This wave is predicted at mooring 15 as well.

The water levels predicted by the stratified numerical model are displayed as dashed lines in Figure 5. The amplitude at mooring 16 is too high but the timing is in good agreement with the observations. The amplitude is better at Eugene Isle, but there is a phase lag of 7 hours. Consequently, the model predicts a maximum along-shelf water surface slope at 0300 UT, August 26, when the observed water level was positive at both locations. In fact, the actual peak surface slope occurred 7 hours earlier and was smaller than predicted. This error may partly be attributable to the 8 m minimum depth and 5 km resolution of the coastline, although similar results have been produced with a model that resolves the coastline (B. Galperin, personal communication, 1998).

The model-predicted phase speed of the barotropic Kelvin wave can be calculated from Figure 5. The peak water level at Eugene Isle occurred 10 hours later than at mooring 16. The phase speed for this barotropic wave is only 2.8 m s^{-1}. This propagation speed is much lower than the speed of 14 m s^{-1} estimated in section 2.3. The low value suggests that the barotropic wave predicted by the model is not freely propagating but is instead being forced (opposed) by the westerly wind stress at the coast.

Model-predicted water surface deviations (Figure 8) reveal the coastally trapped wave inferred from the time series. As the eye approached the eastern moorings (Figure 8a), the geostrophic and the wind forces both had a westward component beneath the wave crest and hindcast flow is predominantly barotropic landward of mooring 14 (compare Figures. 9a and 10a). Flow beneath the trough is weakly anticyclonic near the coast. Several hours after the eye passed over the eastern moorings, the model-predicted trough (Figure 8b) has deepened to more than -1.4 m, while the crest exceeds 1.4 m in elevation. The resulting geostrophic flows (Figures 9b and 10b) on the inner shelf are in opposition to each other. These coastal flows converge west of the storm track to form a southward flowing barotropic jet. The crest of the model-predicted barotropic wave (Figure 8c) propagates less than 30 km at the coast before landfall. The barotropic wave has propagated farther westward at its seaward margin. As seen from the discussion of Figure 5, surface deviations should be positive all along the coast at this time. Several hours after landfall (Figure 8d) the model-predicted storm surge relaxes and propagates as a barotropic Kelvin wave. Eastward barotropic flow on the inner shelf (Figures 9d and 10d) persists, despite the opposing geostrophic forcing beneath the wave crest. Surface currents near mooring 18 have also increased because of the wind change to westerly.

3.1.3. Near-inertial response. The largest near-inertial temperature response predicted by the model is at the shelf break (Figure 3e). The middle meter shows an initial perturbation at 0000 UT, August 26, and a near-inertial oscillation after one IP. The amplitude of this oscillation is more than 4°C. The response within the mixed layer is much

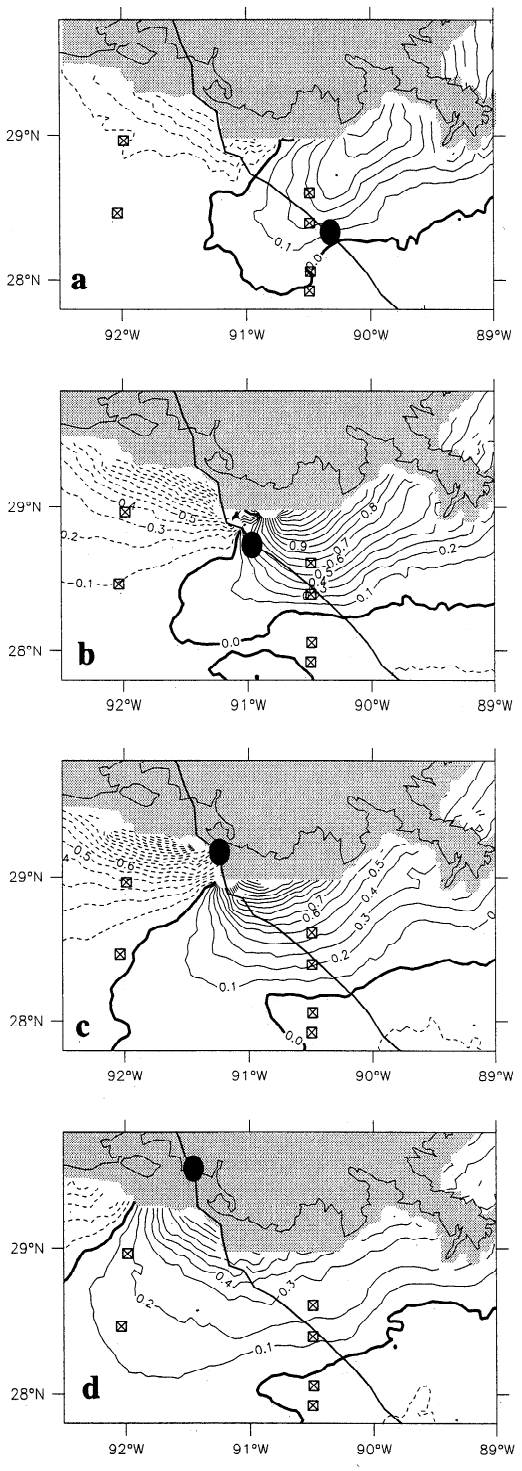

Figure 8. Stratified model results: snapshots of water surface deviation (m) for the Louisiana shelf at (a) 2200 UT, August 25, (b) 0200 UT, August 26, (c) 0600 UT, August 26, and (d) 1000 UT, August 26. The contour interval is 0.1 m. Solid lines are positive deviations, and dashed contours are negative. The location of the eye is indicated by the solid circle.

weaker and is masked by turbulent mixing. There is no evidence of model-predicted near-inertial oscillations in the temperature records at the other moorings.

The near-inertial response dominates surface currents in deep water east of the moorings (Figure 9). Near-inertial currents are predicted near the 200 m isobath within Mississippi Canyon (Figures 9c and 10c). These are identifiable because they point upslope, toward the delta.

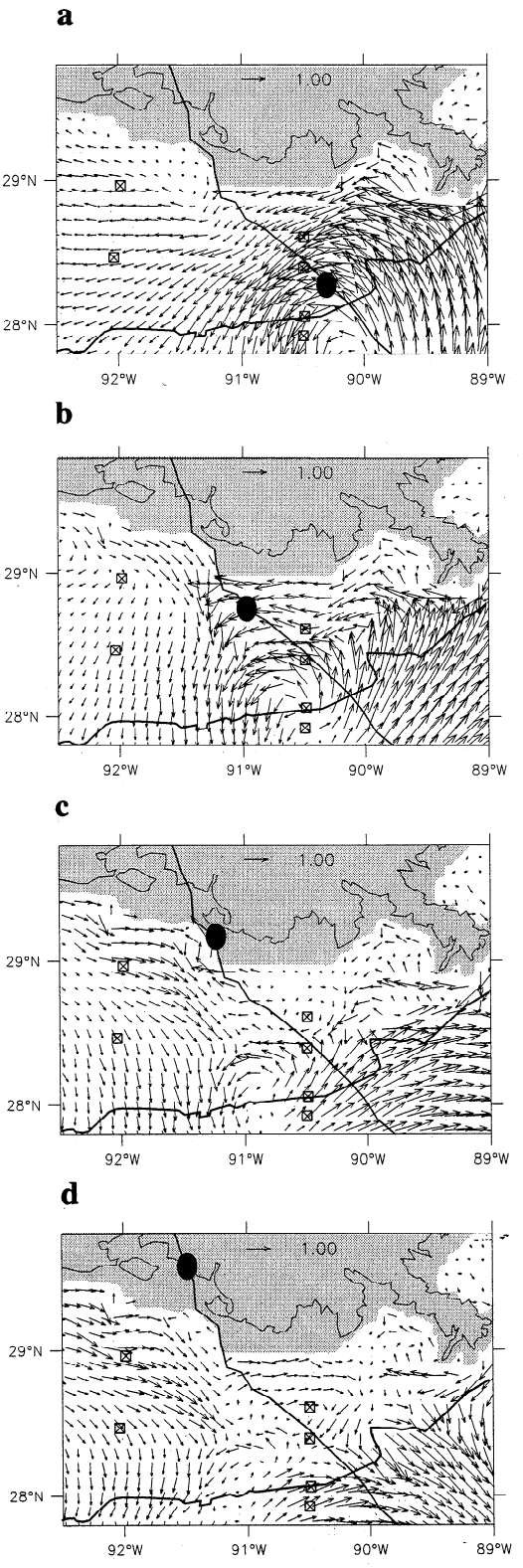

Figure 9. Stratified model results: snapshots of surface currents (m s^{-1}) at (a) 2200 UT, August 25, (b) 0200 UT, August 26, (c) 0600 UT, August 26, and (d) 1000 UT, August 26. The location of the eye is indicated by the solid circle. The 200 m depth contour is shown by the thin line.

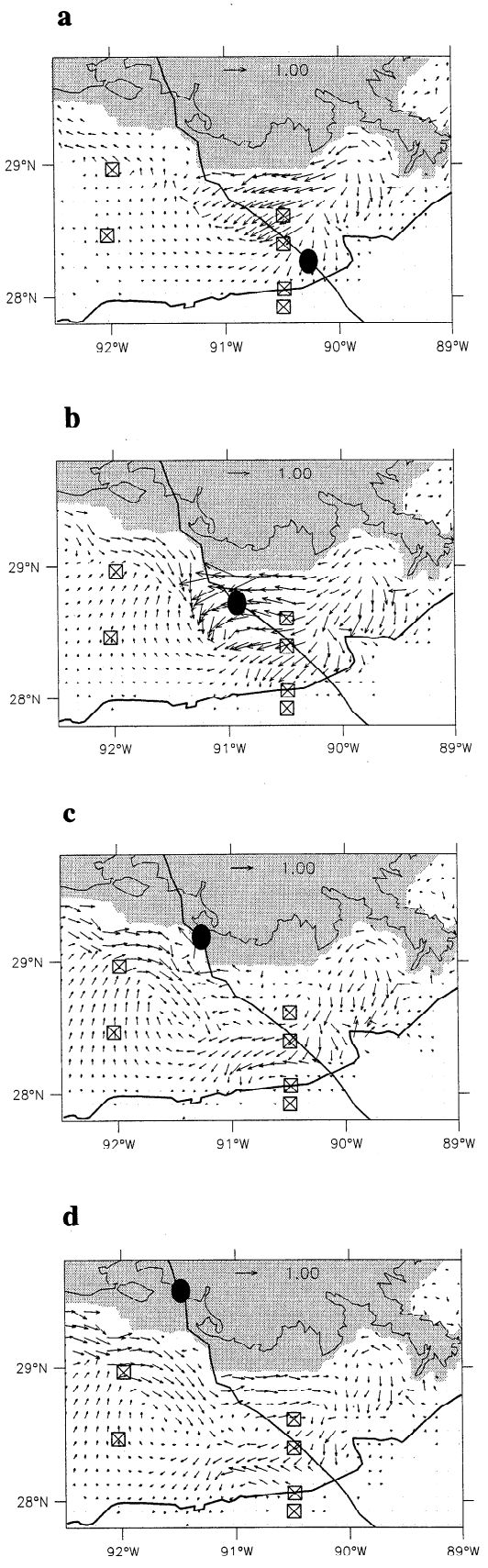

Figure 10. Stratified model results: snapshots of bottom currents (m s^{-1}) at (a) 2200 UT, August 25, (b) 0200 UT, August 26, (c) 0600 UT, August 26, and (d) 1000 UT, August 26. The location of the eye is indicated by the solid circle. The 200 m depth contour is shown by the thin line.

Because of the CCW sense of rotation of the wind vectors west of the storm track, near-inertial oscillations within the mixed layer are not evident in this region during the storm peak. Near-inertial rotation is evident after landfall (Figure 9d) within the mixed layer.

3.1.4. Upwelling and downwelling. The current observations (Figure 4) indicate that downwelling-favorable flow was present at the eastern moorings during the buildup stage of the storm. This flow weakened as surface and bottom currents became more aligned during the directly forced stage. At 2200 UT, August 25, downwelling was still present at mooring 15. A comparison of regional maps of hindcast surface currents (Figure 9a) and bottom currents (Figure 10a) show that this downwelling flow strengthens to the east from the moorings. Bottom currents flow into the eastern margin of Mississippi Canyon (see Figure 6b for location) and exceed 0.5 m s^{-1} near the canyon head. This flow regime continues for another eight hours (Figures 9c and 10c). After landfall (Figures 9d and 10d), downwelling-favorable flow is still present within this region, but currents within the canyon are quite small.

The stratified model accurately predicts the onset of upwelling-favorable flow west of the storm track as the eye approached (Figure 9a and 10a). This flow continues with maximum bottom currents near 0.3 m s^{-1} as the eye made landfall (Figure 10c). After landfall, model-predicted upwelling weakens significantly at mooring 19, while the observations show a shift to a more complex two-layer flow (Figure 4c). The model predicts continued upwelling at mooring 18 as indicated by the measured currents (Figure 4a).

3.2. Unstratified Model Results

Time series of the water levels at mooring 16 and Eugene Isle (Figure 5, solid line) show that the unstratified model is smoother on the shelf than the stratified model during the start-up interval. The maximum water levels are slightly lower. Because of the similarity of the coastal water levels predicted by the two models, therefore, the unstratified model solution is not discussed in this section.

3.2.1. Turbulent mixing. The stratified model has no thermocline to limit turbulent mixing between the surface layer and the deep ocean. Therefore shallow-water currents are predominantly barotropic during much of the hurricane. The surface currents (Figure 11a) as the eye approached the moorings resemble the hurricane wind field. Bottom currents (Figure 12a) are similar, except on the continental slope where they are seaward, although very weak. A cyclonic, barotropic eddy is predicted by the model near the coast at landfall at 90°W (Figures 11c and 12c). Farther offshore, this eddy occurs within the mixed layer only. An anticyclonic eddy is predicted below the mixed layer at the same longitude but at 28.3°N. By 1000 UT, August 26 (Figures 11d and 12d), the eastern mixed layer eddy has intensified, while the deep eddy has weakened. The coastal eddy has dissipated. These eddies show that the unstratified model can simulate the mixed layer and generate two-layer flows, despite the absence of a thermocline.

3.2.2. Coastally trapped waves. Current vectors (Figures 11a and 12a) calculated by the unstratified model are westward, and flow is barotropic beneath the coastal wave crest, as in the stratified model. The eastward barotropic flow on the western side of the storm track converges with the

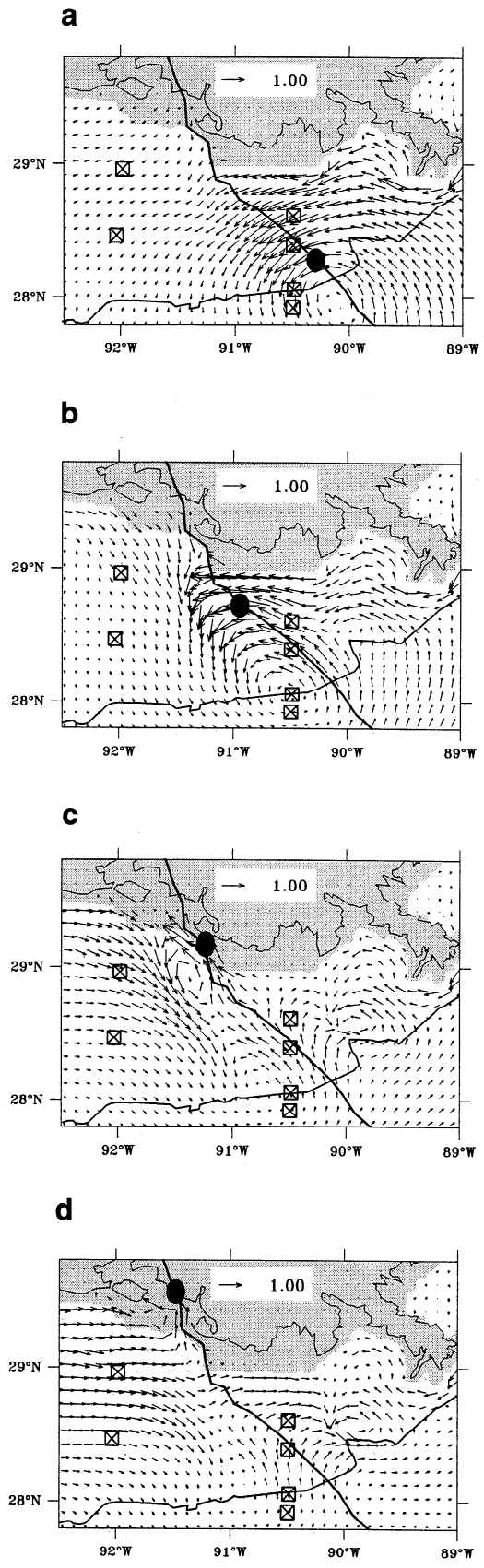

Figure 11. Unstratified model results: snapshots of surface currents (m s^{-1}) at (a) 2200 UT, August 25, (b) 0200 UT, August 26, (c) 0600 UT, August 26, and (d) 1000 UT, August 26. The location of the eye is indicated by the solid circle. The 200 m depth contour is shown by the thin line.

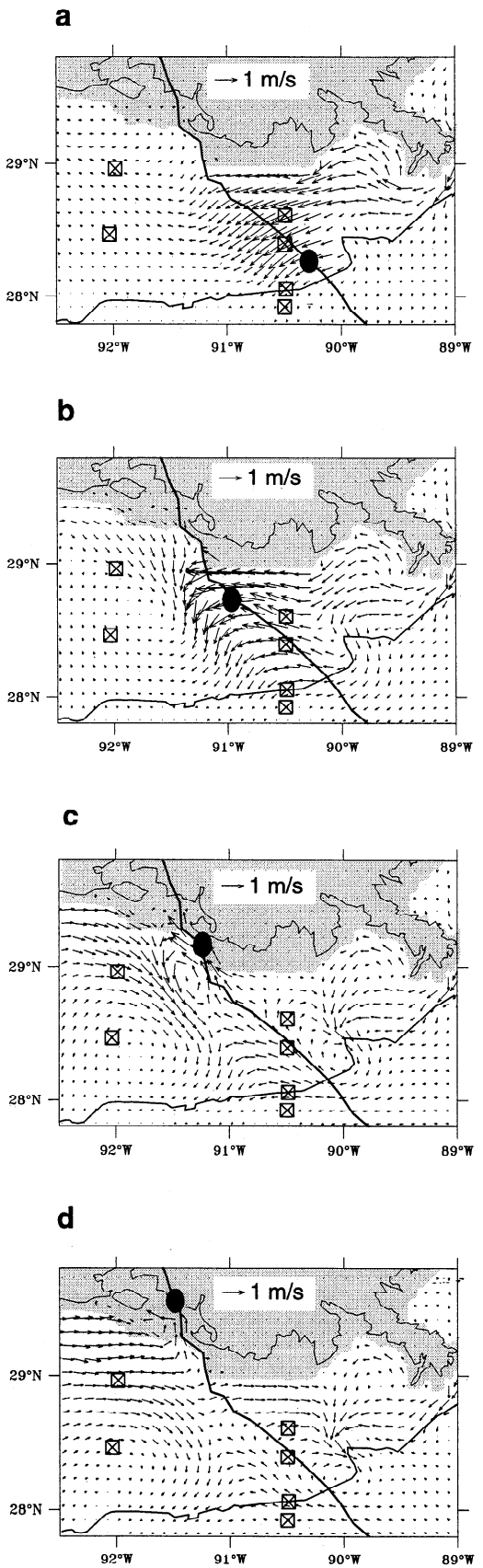

Figure 12. Unstratified model results: snapshots of bottom currents (m s^{-1}) at (a) 2200 UT, August 25, (b) 0200 UT, August 26, (c) 0600 UT, August 26, and (d) 1000 UT, August 26. The location of the eye is indicated by the solid circle. The 200 m depth contour is shown by the thin line.

westward flow from the eastern side to form a barotropic eddy (Figures 11c and 12c) instead of the shear zone predicted by the stratified model. After landfall (Figures 11d and 12d) the forced barotropic wave begins to relax and propagates. Barotropic flow west of the storm track now extends seaward to mooring 19. These currents are forced by the wind stress, which dominates the geostrophic force generated by the wave crest (see Figure 8d). Thus shallow water geostrophic flows associated with the coastal wave tend to be barotropic, but they can be opposed by the wind stress. When this occurs, the flow remains barotropic but follows the dominant forcing.

3.2.3. Near-inertial response. The unstratified model simulates the wind-mixed layer, but because there is no thermocline to restrict momentum transfer to the deep ocean, the near-inertial response of the mixed layer is reduced. Although mixed-layer currents (Figure 11) rotate CW as expected, the rate of rotation is significantly reduced compared to the stratified model (compare Figure 9). The model-predicted bottom currents reveal no apparent near-inertial response.

3.2.4. Upwelling and downwelling. During the approach of the eye to the moorings, bottom currents in the unstratified model (Figure 12a) follow depth contours around the eastern rim of Mississippi Canyon. Several hours later (Figure 12b), downwelling begins at the head of the canyon. These seaward currents turn westward within the canyon to follow isobaths deeper than 200 m. This downwelling is restricted to the canyon and becomes part of a deep-ocean anticyclonic eddy (Figure 12c), until the eddy weakens and downwelling intensifies (Figure 12d). Maximum seaward currents during this final downwelling phase exceed 0.5 m s^{-1}. Shelf-break downwelling never develops in the unstratified model.

As the hurricane eye passed over the eastern moorings, bottom currents (Figures 12b and 12c) near mooring 19 are landward, with very small magnitudes. This upwelling-favorable flow results from weak offshore Ekman transport in the coastal mixed layer.

4. Influence of Stratification

A thermocline was initially present at all of the moorings (Figure 3), and the water column remained partly stratified after the storm. The stratified model computes heat and salinity as prognostic variables and includes full baroclinic effects. It reproduced the temperature time series at the moorings reasonably well. The unstratified model neglects stratification and assumes that density variations are not important for the evolving storm currents.

There are significant differences in the shallow-water currents computed by the stratified and unstratified models. In order to determine the influence of stratification on shallow-water storm currents, the model-predicted currents at the moorings will be compared to the measured storm currents. The following discussion focuses on zonal and meridional current components. Zonal currents (Figure 13) are primarily along shelf, and meridional currents (Figure 14) are mostly across shelf for the Louisiana coast.

4.1. Turbulent Mixing

Previous studies of hurricane circulation were primarily interested in the region near the storm center, where the assumption that the coastal ocean is well mixed is reasonable.

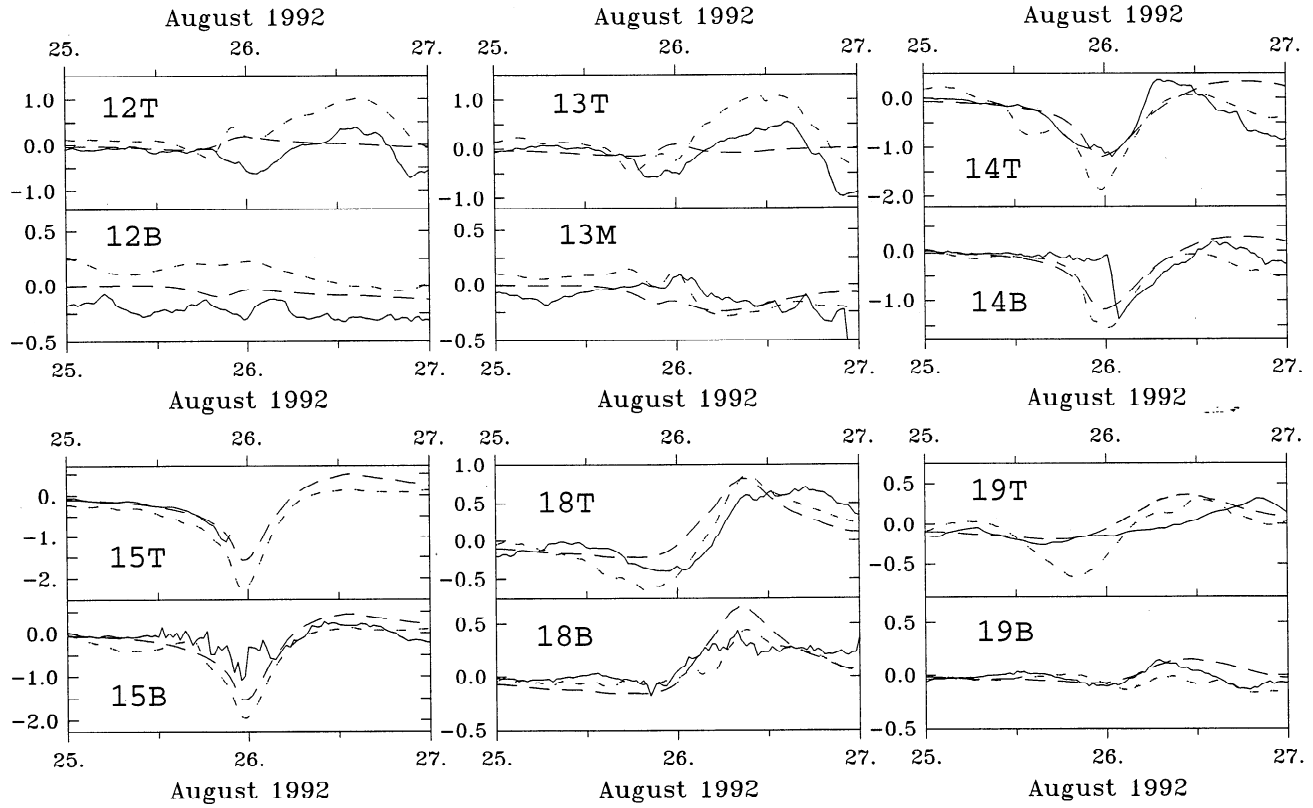

Figure 13. Time series of zonal (east-west) currents at the LATEX moorings listed in Table 1. T, top, B, bottom; solid line, measured; long-dashed line, unstratified; short-dashed line, stratified. See Figure 1 for locations.

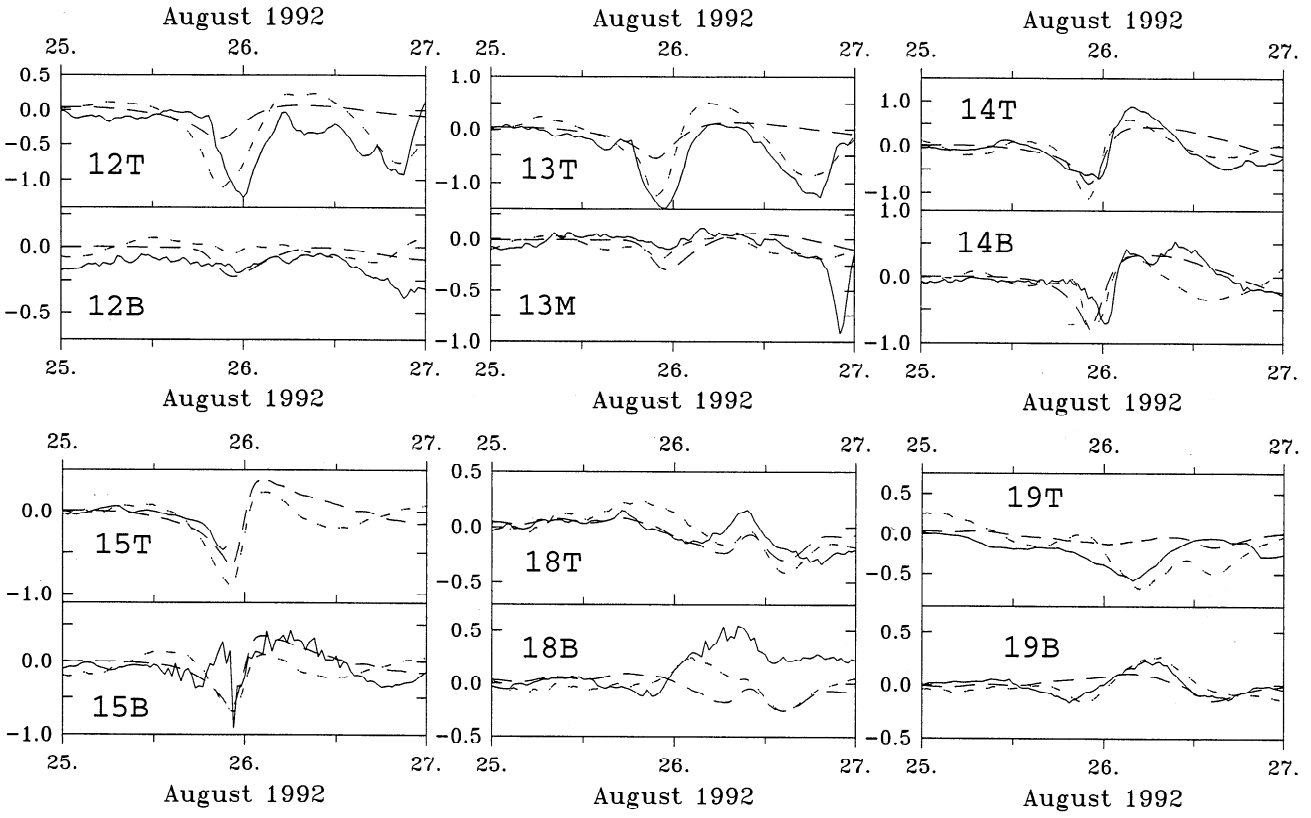

Figure 14. Time series of meridional (north-south) currents at the LATEX moorings listed in Table 1. T, top, B, bottom; solid line, measured; long-dashed line, unstratified; short-dashed line, stratified. See Figure 1 for locations.

For Hurricane Andrew this area would fall within 40 km (1 R_w) to either side of the storm track. Moorings 14 and 15 are within 1 R_w of the storm track in shallow water. Turbulent mixing was strong here, but the stratified model should reproduce these currents if turbulent mixing is correct. Since stratification was significantly reduced, the unstratified model should also accurately simulate the currents at these moorings. In fact, it does better than the stratified model at both upper and lower current meters. The currents predicted by the stratified model are too high, especially for the zonal component.

The unstratified model does a better job within this area partly because of the large uncertainties associated with initial stratification and turbulent mixing under the storm conditions. This performance justifies the use of this kind of model when the primary focus is shallow water near the storm center. Outside this region, however, stratification is not so likely to be destroyed. Where this situation occurs, as at the western moorings, a more complex flow field will evolve.

4.2. Coastally Trapped Waves

The dominant oceanographic response to Hurricane Andrew was the generation of a forced barotropic Kelvin wave (storm surge), which had a major impact on coastal currents near the storm track. This wave was reasonably predicted by both models. The stratified model also predicts temperature changes associated with an internal Kelvin wave on the shelf. Of course, the unstratified model cannot reproduce internal waves, which are dependent on density stratification.

4.3. Near-Inertial Response

The generation of near-inertial oscillations within the mixed layer is an important process at the shelf break and on the slope. This is clearly shown by comparison of the zonal (Figure 13) and meridional (Figure 14) currents at moorings 12 and 13, respectively. These moorings are both within 1 R_w of the storm track. The stratified model captures the dynamics of this response, whereas the unstratified model does not reproduce the near-inertial currents at the deepwater moorings. It should be noted, however, that the unstratified model does simulate a wind-mixed layer.

4.4. Upwelling and Downwelling

One of the most significant differences between the shallow-water current systems predicted by the models is the lack of upwelling and downwelling on the shelf in the unstratified model. Upwelling flow is apparent in the observed meridional currents at the western moorings, and it is predicted by the stratified model. This upwelling is almost nonexistent in the unstratified model. The stratified model predicts downwelling along the shelf east of the moorings and into Mississippi Canyon. Only the canyon flow is predicted by the unstratified model. There are no observations to validate either model in this area, however.

The influence of stratification should be greatest at the western moorings because they were at least 2 R_w from the storm track. The zonal surface currents at moorings 18 and 19 (Figure 13) reflect the changing wind stresses, first being westward (negative) and then reversing to eastward after

landfall on August 16. Both models reproduce the flow at mooring 18, but the stratified model predicts too strong a westward flow on August 25, while the unstratified model predicts too weak a flow. The results at mooring 19 are similar. The meridional currents (Figure 14) near the surface at mooring 18 are predicted slightly better by the unstratified model, but the stratified model does better at the bottom current meter. The homogeneous model does poorly at mooring 19 because it does not predict the observed upwelling flow on August 26. Some of the difficulties seen in both model results at these moorings are very likely attributable to the hindcast wind field. The wind stresses on the left-hand side of the storm, especially for offshore blowing winds, are apparently too large.

5. Summary

Hurricane Andrew crossed the Gulf of Mexico between 1000 UT, August 24, and 0900 UT, August 26, and made landfall on the Louisiana coast after passing over several moored instrument arrays. The resulting data set consists of wind speed and direction, currents, temperature and salinity at different depths within the water column at sites ranging from 500 m to 20 m, and open-ocean water levels near the coast. These data have been used to examine the role of density (temperature) stratification in determining the storm flow in the coastal ocean.

Turbulent mixing was strongest within 1 R_w (radius of maximum winds) of the eye in water depths of 20 m. The water column remained weakly stratified in a water depth of 50 m. Turbulent mixing was much weaker at distances greater than 2 R_w from the storm track.

The dominant coastal response to the hurricane was the generation of a storm surge greater than 0.5 m, east of the storm track, while coastal water levels decreased to almost –1 m west of the storm track. This forced barotropic wave relaxed after the eye made landfall and propagated as a Kelvin wave. There is evidence in the temperature observations of an internal Kelvin wave also, which originated immediately east of the storm track at the coast.

The near-inertial response to the hurricane was very strong on the outer shelf and slope, but there was also a baroclinic wave on the middle shelf. Furthermore, there is evidence of a barotropic near-inertial response in a water depth of 20 m. It is difficult to discern such a weak response near the coast, however, because of the strong barotropic response to the storm surge.

A downwelling-favorable flow regime was present east of the storm track before the storm peak. This flow broke down as turbulent mixing destroyed stratification. An upwelling-favorable flow evolved at more than 2 R_w west of the storm track as the eye made landfall. This flow replaced uniform offshore flow because the barotropic pressure gradient had reached equilibrium with the wind stress for the existing stratification.

Shallow water currents on the Louisiana continental shelf during Hurricane Andrew have been hindcast using the Princeton Ocean Model to simulate three-dimensional (3-D) flow. The build-up and directly forced stages were simulated using both stratified and unstratified models. For regions within 1 R_w of the storm track, the unstratified model predicted shallow-water currents slightly better than the stratified model. At larger distances from the eye, however, where stratification persisted during the storm, the unstratified model was unable to simulate upwelling flows. These flows were reproduced when stratification was included.

Acknowledgments. The first author was funded by the Naval Research Laboratory Very High Resolution 4-D Coastal Ocean Currents project, Program Element 62435N of the Office of Naval Research. The second author was funded by the Middle Atlantic Bight National Undersea Research Center (MAB96-10, NYB94-7) and the Office of Naval Research (N00014-95-1-0457). LATEX mooring data were supplied by the Minerals Management Service (MMS). This work was supported in part by a grant of High Performance Computer (HPC) time from the Department of Defense HPC Shared Resource Centers at the Naval Oceanographic Office and the Army Corps of Engineers Waterways Experiment Station.

References

Blain, C. A., Modeling methodologies for the prediction of hurricane storm surge, in *Recent Advances in Marine Science,* edited by N. Saxena, pp. 177-189, PACON Int., Honolulu, 1997.

Blain, C. A., J. J. Westerink, and R. A. Luettich Jr., Grid convergence studies for the prediction of hurricane storm surge, *Int. J. Numer. Methods Fluids, 26,* 369-401, 1998.

Cardone, V. J., A. T. Cox, J. A. Greenwood, D. J. Evans, H. Feldman, S. M. Glenn, and T. R. Keen, Hindcast study of wind, wave and current fields in Hurricane Andrew, Gulf of Mexico, final report, Miner. Manage. Serv., Herndon, Va., 1994.

Chen, C., and L. Xie, A numerical study of wind-induced, near-inertial oscillations over the Texas-Louisiana shelf, *J. Geophys. Res., 102,* 15,583-15,593, 1997.

Chen C., R. O. Reid, and W. D. Nowlin Jr., Near-inertial oscillations over the Texas-Louisiana shelf, *J. Geophys. Res., 101,* 3509-3524, 1996.

Cooper, C., and B. Pearce, Numerical simulations of hurricane-generated currents, *J. Phys. Oceanogr., 12,* 1071-1091, 1982.

Cooper, C., and J. D. Thompson, Hurricane-generated currents on the outer continental shelf, 1, Model formulation and verification, *J. Geophys. Res., 94,* 12,513-12,539, 1989.

Craig, P. D., and M. L. Banner, Modeling wave-enhanced turbulence in the ocean surface layer, *J. Phys. Oceanogr., 24,* 2546-2559, 1994.

Crepon, M., and C. Richez, Transient unsettling generated by two-dimensional atmospheric forcing and variability in the coastline, *J. Phys. Oceanogr., 12,* 1437-1457, 1982.

Fandry, C. B., and R. K. Steedman, Modelling the dynamics of the transient, barotropic response of continental shelf waters to tropical cyclones, *Cont. Shelf Res., 14,* 1723-1750, 1994.

Fandry, C. B., L. M. Leslie, and R. K. Steedman, Kelvin-type coastal surges generated by tropical cyclones, *J. Phys. Oceanogr., 14,* 582-593, 1984.

Forristall, G. Z., A two-layer model for hurricane-driven currents on an irregular grid, *J. Phys. Oceanogr., 10,* 1417-1438, 1980.

Forristall, G. Z., R. C. Hamilton, and V. J. Cardone, Continental shelf currents in tropical storm Delia: Observations and theory, *J. Phys. Oceanogr., 7,* 532-546, 1977.

Gordon, R. B., Coastal ocean current response to storm winds, *J. Geophys. Res., 87,* 1939-1951, 1982.

Greatbatch, R. J., On the response of the ocean to a moving storm: Parameters and scales, *J. Phys. Oceanogr., 14,* 59-78, 1984.

Harris, D. L., Meteorological aspects of storm surge generation, *J. Hydraul. Eng., 84,* 1-25, 1958.

Hazelworth, J. B., Water temperature variations resulting from hurricanes, *J. Geophys. Res., 73,* 5105-5123, 1968.

Hearn, C. J., and P. E. Holloway, A three-dimensional barotropic model of the response of the Australian north west shelf to tropical cyclones, *J. Phys. Oceanogr., 20,* 60-80, 1990.

Keen, T. R., and S. M. Glenn, A coupled hydrodynamic-bottom boundary layer model of Ekman flow on stratified continental shelves, *J. Phys. Oceanogr., 24,* 1732-1749, 1994.

Keen, T. R., and S. M. Glenn, A quantitative skill assessment of numerical hydrodynamic models of coastal currents, in *Estuarine and Coastal Modeling,* vol. IV, edited by M. L. Spaulding and R. T. Cheng, Am. Soc. of Civ. Eng., *1,* 26-40, 1996.

Keen, T. R., and S. M. Glenn, Factors influencing hindcast skill for modeling shallow water currents during Hurricane Andrew, *J. Atmos. Oceanic Technol., 15*, 221-236, 1998.

Keen, T. R., and R. L. Slingerland, A numerical study of sediment transport and event bed genesis during Tropical Storm Delia, *J. Geophys. Res., 98*, 4775-4791, 1993a.

Keen, T. R., and R. L. Slingerland, Four storm-event beds and the tropical cyclones that produced them: a numerical hindcast, *J. Sediment. Petrol., 63*, 218-232, 1993b.

LeBlond, P. H., and L. A. Mysak, *Waves in the Ocean*, 602 pp., Elsevier, New York, 1978.

Mellor, G. L., *Users Guide for a Three-Dimensional, Primitive Equation, Numerical Ocean Model*, 35 pp., Inst. of Nav. Oceanogr., Princeton Univ., Princeton, N. J., 1993.

Mellor G. L., and T. Yamada, Development of a turbulence closure model for geophysical fluid problems, *Rev. Geophys., 20*, 851-875, 1982.

Murray, S. P., Bottom currents near the coast during Hurricane Camille, *J. Geophys. Res., 75*, 4579-4582, 1970.

Niwa, Y., and T. Hibiya, Nonlinear processes of energy transfer from traveling hurricanes to the deep ocean internal wave field, *J. Geophys. Res., 102*, 12,469-12,477, 1997.

Oey, L, and P. Chen, A nested-grid ocean model: With application to the simulation of meanders and eddies in the Norwegian coastal current, *J. Geophys. Res., 97*, 20,063-20,086, 1992.

Shay, L. K., and S. W. Chang, Free surface effects on the near-inertial ocean current response to a hurricane: A revisit, *J. Phys. Oceanogr., 27*, 23-39, 1997.

Shay, L. K., S. W. Chang, and R. L. Elsberry, Free-surface effects on the near-inertial ocean current response to a hurricane, *J. Phys. Oceanogr., 20*, 1405-1424, 1990.

Signorini, S. R., J. S. Wei, and C. D. Miller, Hurricane-induced surge and currents on the Texas-Louisiana shelf, *J. Geophys. Res., 97*, 2229-2242, 1992.

Smith, N. P., Longshore currents on the fringe of Hurricane Anita, *J. Geophys. Res., 83*, 6047-6051, 1978.

Smith, N. P., Response of Florida Atlantic shelf waters to Hurricane David, *J. Geophys. Res., 87*, 2007-2016, 1980.

Spaulding, M. L., and T. Isaji, Three dimensional continental shelf hydrodynamics model including wave current interaction, in *Three-Dimensional Models of Marine and Estuarine Dynamics*, edited by J. C. J. Nihoul and B. M. Jamart, pp. 405-426, Elsevier, New York, 1987.

Swift, D. J. P., J. P. Han, and C. E. Vincent, Fluid processes and sea floor response on a modern storm-dominated shelf: Middle Atlantic shelf of North America, I, The storm current regime, in *Shelf Sands and Sandstone Reservoirs*, edited by R. J. Knight and J. R. McClean, pp. 99-109, Mem. 11, Can. Soc. of Petrol. Geol., Calgary, 1986.

Tang, Y. M., and R. Grimshaw, A modal analysis of coastally trapped waves generated by tropical cyclones, *J. Phys. Oceanogr., 25*, 1577-1598, 1996.

Tang, Y. M., P. Holloway, and R. Grimshaw, A numerical study of the storm surge generated by tropical cyclone Jane, *J. Phys. Oceanogr., 27*, 963-976, 1997.

S. M. Glenn, Institute of Marine and Coastal Sciences, Rutgers University, New Brunswick, NJ 08903.

T. R. Keen, Naval Research Laboratory, Oceanography Division, Stennis Space Center, MS 39529. (e-mail:keen@nrlssc.navy.mil)

(Received May 26, 1997; revised March 17, 1999; accepted May 19, 1999.)